

# Forecasting sudden changes in environmental pollution patterns

María J. Olascoaga<sup>a,1</sup> and George Haller<sup>b,c</sup>

<sup>a</sup>Rosenstiel School of Marine and Atmospheric Science, University of Miami, 4600 Rickenbacker Cswy., Miami, FL 33149; <sup>b</sup>Department of Mechanical Engineering, McGill University, 817 Sherbrooke Avenue West, Montreal, Quebec H3A 2K6, Canada; and <sup>c</sup>Department of Mathematics and Statistics, McGill University, 817 Sherbrooke Avenue West, Montreal, Quebec H3A 2K6, Canada

Edited by Alexandre J. Chorin, University of California, Berkeley, CA, and approved February 3, 2012 (received for review November 10, 2011)

The lack of reliable forecasts for the spread of oceanic and atmospheric contamination hinders the effective protection of the ecosystem, society, and the economy from the fallouts of environmental disasters. The consequences can be dire, as evidenced by the *Deepwater Horizon* oil spill in the Gulf of Mexico in 2010. We present a methodology to predict major short-term changes in environmental contamination patterns, such as oil spills in the ocean and ash clouds in the atmosphere. Our approach is based on new mathematical results on the objective (frame-independent) identification of key material surfaces that drive tracer mixing in unsteady, finite-time flow data. Some of these material surfaces, known as Lagrangian coherent structures (LCSs), turn out to admit highly attracting cores that lead to inevitable material instabilities even under future uncertainties or unexpected perturbations to the observed flow. These LCS cores have the potential to forecast imminent shape changes in the contamination pattern, even before the instability builds up and brings large masses of water or air into motion. Exploiting this potential, the LCS-core analysis developed here provides a model-independent forecasting scheme that relies only on already observed or validated flow velocities at the time the prediction is made. We use this methodology to obtain high-precision forecasts of two major instabilities that occurred in the shape of the *Deepwater Horizon* oil spill. This is achieved using simulated surface currents preceding the prediction times and assuming that the oil behaves as a passive tracer.

In April 2010, a blowout caused an explosion on the *Deepwater Horizon* (DWH) mobile offshore oil rig near the Mississippi River's mouth in the Gulf of Mexico. The resulting fire could not be extinguished and the drilling rig sank shortly after, leaving the oil well gushing at the sea floor. Before the well was capped in mid-July, an estimated 4 million barrels of oil escaped (1), causing the largest accidental marine oil spill in the history of the petroleum industry. Beyond the enormous ecological damage, the spill resulted in an estimated loss of over a billion dollars for the tourism industry alone.

In this environmental disaster, uncertainties in the spread of the pollutant plume had severe financial implications. Mass cancellations devastated the tourism industry along the Southwest Florida coastline, which was never actually reached by the DWH oil spill. Beyond the measurable cost, the lack of reliable forecasts for the spread of contamination hindered effective countermeasures and led to suboptimal resource allocation by decision makers.

Precise longer-term forecasts for the underlying ocean flow have not been within reach because of the same inherent sensitivities and uncertainties that affect weather-forecasting models. Shorter-term predictions of ocean currents are more accurate, but the relevant details of such predictions typically depend on the models and initial conditions on which they are based.

In this paper, we propose an approach to short-term (4–6 d) prediction of impending changes in the material distribution of a pollutant plume in the ocean, as opposed to the current practice of forecasting changes in the full unsteady velocity field. Our methodology assumes that time-resolved measured velocities or validated model velocities are available up to the present time

when the forecast is made. No assumption is made, however, about the availability of future velocities from numerical models.

Our approach is Lagrangian (i.e., fluid-trajectory based), and takes advantage of modern developments in nonlinear dynamical systems theory. In particular, we use Lagrangian coherent structures (LCSs), the recently discovered hidden skeleton behind complex mixing patterns in unsteady flows (2, 3), to make short-term predictions of major deformations that are about to happen in an observed tracer pattern. What makes this possible is the structural stability of LCSs with highly attracting cores, which generate enough momentum to keep the tracer on its pathway for a while, even if unexpected or unresolved perturbations arise from the underlying velocity field. The resulting methodology, LCS-core analysis, is based on exact mathematical results, frame independent, and does not rely on future model data. These features differentiate it from other proposed Lagrangian approaches (see, e.g., ref. 4) and enable highly localized predictions for short-term tracer instabilities without the danger of false positives or negatives.

We illustrate the proposed methodology by forecasting the location and time of two main instabilities that had a crucial impact on the shape of the DWH oil spill. The first such event, the “tiger-tail” instability, took place on May 17, 2010. It involved an unexpected southeastward spread of the spill, in the form of a prominent finger, into a cyclonic eddy north of a much larger anticyclonic eddy pinched off from the Loop Current. The second event we forecast is the “coastal-spread” instability, an inward bend of the spill along the northwestward direction around June 10, 2010, followed by a southwestward-northeastward elongation that led to the accumulation of oil along the northeastern Gulf of Mexico coastline.

Our analysis of the DWH oil spill is based on surface velocity fields obtained from a general ocean circulation model that assimilates in situ observations and satellite-based remote sensing. In these forecasts, we neglect nonconservative behavior, such as diffusive mixing of the oil and chemical reactions, as well as sub-mesoscale processes whose length scales (less than 10 km) are well-separated from the large-scale instabilities we seek to forecast. Even with these approximations, we obtain remarkably accurate predictions of instabilities in the shape of the spill, which underlines the robustness of the LCS-core analysis developed here.

## Results and Discussion

**Tracer Instabilities in Steady and Unsteady Flows.** Two-dimensional incompressible fluid motion is governed by the differential equation

$$\dot{x} = v(x, t), \quad \nabla \cdot v = 0, \quad [1]$$

where the overdot denotes differentiation with respect to the time  $t$ ,  $\nabla$  denotes the gradient with respect to the two-dimensional spatial

Author contributions: M.J.O. and G.H. designed research; M.J.O. and G.H. performed research; M.J.O. and G.H. contributed new reagents/analytic tools; and M.J.O. and G.H. wrote the paper.

The authors declare no conflict of interest.

This article is a PNAS Direct Submission.

<sup>1</sup>To whom correspondence should be addressed. E-mail: jolascoaga@rsmas.miami.edu.



to unsteady, finite-time flow data. In particular, hyperbolic regions attract material along a pathway transverse to the attracting LCS, then eject the attracted material along the LCS.

Unlike saddle points in steady flows, however, hyperbolic regions are dynamic and transient in nature: they form, travel with the flow then disappear. The formation of a hyperbolic region is a precursor to one of the two types of tracer instabilities shown in Fig. 1 *B* and *C*, depending on its location relative to the tracer blob of interest.

As shown in ref. 10, the instantaneous normal attraction rate of an LCS at a point  $x_t$  with unit normal  $n_t$  is measured by the Lagrangian strain rate

$$r(x_t, t) = \langle n_t, S(x_t, t)n_t \rangle, \quad [4]$$

where  $S = \frac{1}{2}[\nabla v + (\nabla v)^*]$  is the rate-of-strain tensor evaluated in 4 along the backward fluid trajectory  $x_t = F_t^t(x_0)$  for times  $t \leq t_0$ . Substituting the expression  $n_t = [\nabla F_t^{t_0}(x_t)]^* n_0 / |[\nabla F_t^{t_0}(x_t)]^* n_0|$  from ref. 7 into Eq. 4 and using the fact that  $n_0 = \xi_2(x_0)$  holds along an LCS, we obtain

$$r(x_t(x_0), t) = \frac{\langle \xi_2(x_0), \tilde{S}(x_t(x_0), t)\xi_2(x_0) \rangle}{|[\nabla F_t^{t_0}(x_t(x_0))]^* \xi_2(x_0)|^2}, \quad [5a]$$

where

$$\tilde{S}(x_t(x_0), t) = \nabla F_t^{t_0}(x_t(x_0))S(x_t(x_0), t)[\nabla F_t^{t_0}(x_t(x_0))]^* \quad [5b]$$

and the notation  $x_t(x_0)$  is used to point out the dependence of the backward position  $x_t$  on the present position  $x_0$ . We conclude that a fluid trajectory  $x_t$  in an attracting LCS lies within a uniformly hyperbolic region over a time interval  $[t_0 - T, t_0]$  if the strain rate  $r(x_t(x_0), t)$  listed in 5a stays negative for all  $t$  values in  $[t_0 - T, t_0]$ . Such  $x_t$  trajectories form the core of an attracting LCS, playing the role of generalized saddle points in the tracer instabilities shown in Fig. 1. To identify the most influential LCS cores at the prediction time  $t_0$ , we additionally require  $|r(x_0, t_0)|$  to be large relative to strain rates of other LCS cores (cf. *Methods*). Monitoring the emergence of LCS cores inside and outside a tracer pattern, such as an evolving oil spill, therefore provides us with a prediction tool (LCS-core analysis) for imminent shape changes in the pattern, without any reliance on future velocity data.

**Application to DWH Oil Spill Instabilities.** Here we show how LCS-core analysis predicts the formation of two major instabilities in the DWH oil spill. In particular, we capture two key LCS cores, stronger than 99% of coexisting LCS cores, that foretell the tiger-tail and coastal-spread instabilities 4–6 d before they are actually observed around May 17, 2010 and June 15, 2010, respectively. Snapshots recording the development of these instabilities in the observed oil spill are shown in Fig. 3.

The results of LCS-core analysis applied to the tiger-tail instability are shown in Fig. 4. For each time  $t_0$ , the corresponding panel shows the strongest (top 1%) uniformly hyperbolic regions as circles overlaid on the silhouette of the observed oil slick. Double-headed arrows indicate the predicted direction of maximum Lagrangian stretching, marked by  $\xi_1(x_0)$ , at the center of each circle. The length of these arrows is scaled by  $\sqrt{\lambda_2(x_0)}$ , the local normal repulsion rate of the LCS containing  $x_0$  (7).

Two LCS cores are identified whose strengths remain moderate from April 30, 2010 through May 2, 2010, predicting the lack of any imminent large-scale instability (Fig. 4A). Observe, however, the smaller-scale inward fingers created by the LCS core outside the perimeter of the spill, in agreement with our earlier sketch in Fig. 1C. These smaller instabilities need virtually no time to build up: They involve smaller masses of oil and water, reacting instantaneously to the presence of relatively weak hyperbolic cores. Our description of them, therefore, cannot be considered forecasting but, rather, now-casting. Still, the accuracy

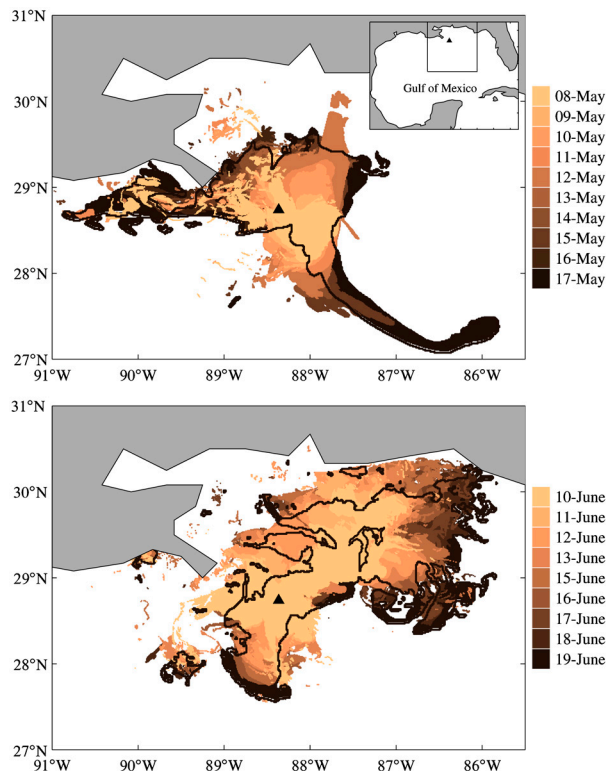


**Fig. 3.** Snapshots from the periods May 8, 2010–May 17, 2010 (*Upper*) and June 10, 2011–June 19, 2011 (*Lower*), showing observed oil distribution on the surface of the northern Gulf of Mexico. The black curve in each panel indicates the silhouette of the oil slick on the last day shown. The box in the inserted map in the *Upper* panel shows the specific area under study. The triangle in each map indicates the DWH oil spill site.

of our scheme in locating the root causes of these small-scale inward fingering events is notable.

Next note that the strength of one of the LCS cores increases significantly from May 9, 2010 through May 13, 2010, signaling an impending large-scale instability (Fig. 4B). As time progresses, the direction of maximum Lagrangian stretching rotates anticlockwise, forecasting the direction along which the oil eventually breaks away and acquires the tiger-tail-shaped distribution on May 17, 2010. This major instability is, therefore, signaled by our LCS-core analysis about 1 wk before its full development. This is because a large-scale tracer instability that goes beyond small filament formation needs time to build up, as the large masses of water and oil involved gradually gain momentum.

We now document the role of the attracting LCS, whose core is shown in Fig. 4B, in the further development of the tiger-tail instability. Fig. 5 shows snapshots of the evolving spill, with all attracting LCSs overlaid, and with synthetic fluid particle positions (blue) initially lying within the LCS core identified on May 11, 2010. Gradually, the patch of blue particles spreads and forms the approximate centerpiece of the tiger-tail-shaped finger on May 17, 2010. Remarkably, whereas diffusion, windage, three-dimensionality, and other effects cause the spill to divert from its LCS skeleton, the continued overall relevance of the LCS in shaping the spill is evident from Fig. 5. As in the case of the tiger-tail instability, the results of our LCS-core analysis are shown in Fig. 6 for the coastal-spread instability. In this case, one or two strong hyperbolic cores are uncovered each day of the week that precedes the full development of the instability. The eventual push of the spill towards the coast (Fig. 6, *Upper*) is forecasted by growing Lagrangian strain around June 7, 2010. The subsequent spread along the coastline (Fig. 6, *Lower*) is now-casted





LCS-core analysis is broadly applicable to contamination spread in geophysical flows. We recall the 2010 eruption of Eyjafjallajökull, an ice-covered volcano in Iceland, which threw ash several kilometers up in the atmosphere. This resulted in widespread airspace closure in western and northern Europe for a period of 6 d. Beyond the major inconvenience to would-be travelers on about 95,000 canceled flights, the shutdown caused an estimated \$1.7 billion loss for the airspace industry globally (18). All this has motivated an ongoing LCS-core analysis of instabilities in the 2010 ash pattern. The results of that study will be reported elsewhere. We also mention red tides produced by the accumulation of toxic dinoflagellates near the surface of the ocean. In particular, red tides constitute a recurrent problem along the Florida's west coast with negative effects for the health of marine ecosystems as well as human health and, consequently, the regional economy (20). LCS-core analysis can be applied to investigate instabilities in the shape of a red tide distribution once developed.

## Methods

**Dataset.** The numerically generated velocity data employed in our analysis of the DWH oil spill consists of daily surface ocean currents produced by the experimental real-time Intra-Americas Sea Nowcast/Forecast System (IASNF), which is based on the NCOM. The model has 0.04°-horizontal-resolution (roughly 3.5 km at mid latitudes), and 41 terrain-following ( $\sigma$ ) levels. The model's topography is taken from the Naval Research Laboratory 2-min digital bathymetry database. The model assimilates satellite-observed sea-surface height anomalies, sea-surface temperature, and a suite of available in situ observations. Surface forcing is applied using surface heat fluxes, including solar radiation, wind stresses and sea level air pressure from the Navy Operational Global Atmospheric Prediction System and US Navy Fleet Numerical Meteorology and Oceanography Center database. The open boundary conditions, including sea-surface elevation, transport, temperature, salinity, and currents are provided by the NRL 0.08°-resolution global NCOM, which is operated daily. The model also incorporates monthly discharges from 140 rivers. More information can be found at [http://www7320.nrlssc.navy.mil/IASNFS\\_WWWW](http://www7320.nrlssc.navy.mil/IASNFS_WWWW) and in the references cited there.

The surface oil images used in our analysis were produced by the National Oceanic and Atmospheric Administration (NOAA) Experimental Marine Pollution Surveillance Reports (EMPSR). The EMPSR, which were constructed by NOAA during the DWH oil spill, delineated the extent of surface oil using satellite imagery from both active and passive sensors, and from other supplementary information, such as overflights and in situ observations. More information can be obtained at <http://www.ssd.noaa.gov/PS/MPS/deepwater.html>.

**Computational Aspects of LCS-Core Analysis.** Our computational domain is within a circle  $\mathcal{C}$  of radius 200 km centered at the oil well. Starting from  $\mathcal{C}$  at each base time  $t_0$ , we compute backward-time fluid trajectories by solving the differential Eq. 1, with initial conditions distributed over a regular grid of 0.004° resolution. In solving 1, we employ a variable time-step, fourth/fifth-order Runge–Kutta integration scheme, with the required spatiotem-

poral interpolations performed using a linear method. The backward integration time we use is  $T = 15$  d \*, starting from the running present time  $t_0$  at which we make our predictions. As mentioned earlier, we use no future model velocities beyond what is already available and have been validated by time  $t_0$ .

The Cauchy–Green strain tensor field and its invariants are computed from finite-differencing over initial particle positions, and from exact pointwise formulae for the strain eigenvalue  $\lambda_2$  and eigenvector  $\xi_2$ . Because of the higher numerical stability of  $\xi_2$ , we compute  $\xi_1$  as a vector orthonormal to  $\xi_2$ . Next, we identify the subset  $\mathcal{C}_0$  of the circular domain  $\mathcal{C}$  on which condition 3 holds, then compute strainlines within  $\mathcal{C}_0$  by solving the differential Eq. 2 via a fixed-step fourth-order Runge–Kutta scheme. While 2 is time independent, accurate strainline computation is challenging because of inherent orientational discontinuities and degenerate points that exist in the eigenvector field of the tensor field  $C_{t_0}^{t_0-T}(x_0)$ . These challenges have been addressed for general tensor lines in the scientific visualization literature (see, e.g., ref. 21) and can be adapted to our present context (9). As a result, however, the strainline segments will no longer be parametrized by arc length, and hence the average repulsion rate along them should be computed as  $\bar{\lambda}_2(\gamma_0) = (\int_{\gamma_0} \lambda_2(x_0(s)) |x_0'(s)| ds) / \text{length}(\gamma_0)$ .

Attracting LCSs at the current time  $t_0$  are identified as strainlines  $\gamma_0$  in  $\mathcal{C}_0$  that locally maximize the average repulsion rate  $\bar{\lambda}_2(\gamma_0)$ . We identify such strainlines by intersecting all strainlines in  $\mathcal{C}_0$  with a set of longitudinal and latitudinal lines spaced 0.25° apart, then identifying the locations at which  $\bar{\lambda}_2(\gamma_0)$  exhibits a local maximum along at least one member of the selected set of lines (see ref. 9 for more detail). Having extracted all attracting LCS at the time  $t_0$  in this fashion, we identify their cores by detecting their points satisfying  $r(x_t(x_0), t) < 0$  for all  $t \in [t_0 - T, t_0]$ .

To focus on predicting the most robust instabilities, we only use the strongest 1% of all LCS-core points detected in this fashion, with their strength characterized by  $|r(x_0, t_0)| = \langle \xi_2(x_0), S(x_0, t_0) \xi_2(x_0) \rangle$ . Weaker LCS cores also participate in shaping the spill, but their prediction is less reliable given their sensitivity to changes in the wind field, unresolved smaller scales, and three-dimensional effects.

**ACKNOWLEDGMENTS.** Critical reading of the paper by Francisco J. Beron-Vera is sincerely appreciated. We thank Joaquin A. Trianes for producing and making available to us digitized versions of the observed surface ocean oil distribution images available at <http://www.ssd.noaa.gov/PS/MPS/deepwater.html>. Original image data were processed by the Center for Southeastern Tropical Advanced Remote Sensing of University of Miami. M.J.O. was supported by the National Science Foundation under Grant CMG0825547 and OCE0432368/0911373/1127813, National Institute of Environmental Health Sciences under Grant P50 ES12736, National Aeronautics and Space Administration Grant NNX10AE99G, and by a grant from British Petroleum/The Gulf of Mexico Research Initiative. G.H. was supported by the Canadian Natural Sciences and Engineering Research Council under Grant 401839-11.

\*The choice of the time scale  $T$  is informed by the need to detect LCSs of the size of interest (a few tens of kilometers), while excluding highly convoluted smaller flow features that obscure the analysis. This can be anticipated by noting that 15 d is roughly twice the turnover time scale estimated for mesoscale eddies. For instance, for an eddy radius and tangential velocity of 75 km and 0.1 ms<sup>-1</sup>, respectively, the eddy-turnover time scale is about 8 d. Other studies involving LCS identification in the Gulf of Mexico employed similar Lagrangian integration time choices (12, 16, 19, 20).

- Crone TJ, Tolstoy M (2010) Magnitude of the 2010 Gulf of Mexico oil leak. *Science* 330:634.
- Haller G (2000) Finding finite-time invariant manifolds in two-dimensional velocity fields. *Chaos* 10:99–108.
- Peacock T, Dabiri J (2010) Introduction to focus issue: Lagrangian Coherent Structures. *Chaos* 20:017501.
- Mézic IS, Loire VAF, Hogan P (2010) A new mixing diagnostic and the Gulf of Mexico oil spill. *Science* 330:489.
- Arnold VI (1989) *Mathematical Methods of Classical Mechanics* (Springer, New York), 2nd Ed.
- Haller G, Poje AC (1998) Finite time transport in aperiodic flows. *Physica D* 119:352–380.
- Haller G (2011) A variational theory of hyperbolic Lagrangian Coherent Structures. *Physica D* 240:574–598.
- Farazmand M, Haller G (2011) Erratum and addendum to a variational theory of hyperbolic Lagrangian coherent structures. *Physica D* 240:574–598 and erratum (2011) 241:439–441.
- Farazmand M, Haller G (2012) Computing hyperbolic lagrangian coherent structures from variational lcs theory. *Chaos*, in press.
- Haller G (2002) Lagrangian coherent structures from approximate velocity data. *Phys Fluids* 14:1851–1861.
- Koh TY, Legras B (2002) Hyperbolic lines and the stratospheric polar vortex. *Chaos* 12:382–394.
- Olascoaga MJ, Beron-Vera FJ, Brand LE, Koçak H (2008) Tracing the early development of harmful algal blooms on the West Florida Shelf with the aid of Lagrangian coherent structures. *J Geophys Res* 113:C12014.
- Peng J, Peterson R (2012) Attracting structures in volcanic ash transport. *Atmos Environ* 48:230–239.
- Tallapragada P, Ross SD, Schmale DG (2011) Lagrangian coherent structures are associated with fluctuations in airborne microbial populations. *Chaos* 21:033122.
- Huntley HS, Lipphardt B, Kirwan A (2011) Surface drift predictions of the deepwater horizon spill: The lagrangian perspective. *Geophys Monogr Ser* 195:179–195.
- Olascoaga MJ, et al. (2006) Persistent transport barrier on the West Florida Shelf. *Geophys Res Lett* 33:L22603.
- Coulliette C, Lekien F, Paduano J, Haller G, Marsden J (2007) Optimal pollution mitigation in Monterey bay based on coastal radar data and nonlinear dynamics. *Environ Sci Tech* 41:6562–6572.
- Wearden G (April 10, 2010) Ash cloud costing airlines £130M a day. *The Guardian (London)* Business Section.
- Beron-Vera FJ, Olascoaga MJ (2009) An assessment of the importance of chaotic stirring and turbulent mixing on the West Florida Shelf. *J Phys Oceanogr* 39:1743–1755.
- Olascoaga MJ (2010) Isolation on the West Florida Shelf with implications for red tides and pollutant dispersal in the Gulf of Mexico. *Nonlin Proc Geophys* 17:685–696.
- Tchon KF, Dompierre J, Vallet MG, Guibault F, Camarero R (2006) Two-dimensional metric tensor visualization using pseudo-meshes. *Eng Comp* 22:121–131.